Acta Cryst. (1999). A**55**, 267–273

X-ray standing wave as a result of only the imaginary part of the atomic scattering factor

Riichirou Negishi,[a]* Tomoe Fukamachi[a] and Takaaki Kawamura[b]

[a]*Saitama Institute of Technology, Okabe, Saitama 369-0293, Japan, and* [b]*Department of Physics, Yamanashi University, Kofu, Yamanashi 400-8510, Japan. E-mail: negishi@sit.ac.jp*

(*Received 27 January 1997; accepted 9 June 1998*)

Abstract

The X-ray standing wave has been studied when the real part of the scattering factor is zero. In the symmetric Laue case, the phase of the standing wave advances by π when the deviation parameter W changes from -1 to 1, which is the same variation as in the usual symmetric Bragg case when only the real part of the scattering factor exists. However, the phase in the former case is different from that in the latter by $\pi/2$. By using the standing waves, the origins of the anomalous transmission and anomalous absorption effects reported by Fukamachi & Kawamura [*Acta Cryst.* (1993), A**49**, 384–388] have been analysed. The standing wave in the Laue case can give rise to a more accurate method of site determination of a specified impurity atom as well as a wider range of applications than a conventional standing-wave approach.

1. Introduction

The use of X-rays from synchrotron radiation makes it possible to study dynamical diffraction due to anomalous scattering by changing the X-ray energy very near the absorption edge of an atom in a crystal. For example, Fukamachi *et al.* (1993) have observed X-ray dynamical diffraction resulting from only the imaginary part of the Fourier component of the X-ray polarizability (χ_{hi}), *i.e.* when the real part (χ_{hr}) is zero, by measuring the 844 reflection of Ge using synchrotron X-rays at the Photon Factory (KEK-PF). Fukamachi & Kawamura (1993) have rewritten dynamical diffraction intensities in order to treat such an extreme case. They have pointed out several interesting effects expected for dynamical diffraction very near an absorption edge: in the Laue case, for example, the Borrmann effect is expected to be conspicuous, and, in the Bragg case, the rocking curve becomes quite sharp. The latter effect was also pointed out by Kato (1992). Fukamachi *et al.* (1994) have studied rocking curves in the Laue case for large χ_{hi} and pointed out a non-transparent effect for a thin crystal as well as enhanced anomalous transmission in an asymmetric reflection when $\chi_{hr} = 0$.

Recently, Fukamachi *et al.* (1995) studied dispersion surfaces based on a theory by Fukamachi & Kawamura (1993) and pointed out that the dispersion surface for $\chi_{hr} = 0$ is quite different from that for $\chi_{0i} = 0$. They have also shown that the cause of anomalous transmission as well as anomalous absorption in the Laue case for $\chi_{hr} = 0$ is understood intuitively by using the dispersion surface. The cause of the sharpened rocking curve in the Bragg case for $\chi_{hr} = 0$, which was pointed out by Fukamachi & Kawamura (1993), is also understood by looking at the shape of the dispersion surface.

In this paper, we analyse the forms of the standing waves in a crystal for $\chi_{hr} = 0$, which are made up by the transmitted and the diffracted components of the waves in the crystal. The relation of anomalous absorption and transmission to the standing waves is also prescribed.

2. Some basic equations

In this section, we will give some basic equations needed in the analysis that follows; the details are given by Fukamachi & Kawamura (1993). The Fourier transforms of the X-ray polarizability, its real and imaginary components, which consist of the real and the imaginary parts of the atomic scattering factors, are written as

$$\begin{aligned}\chi_h &= \chi_{hr} + i\chi_{hi} \\ &= |\chi_{hr}| \exp(i\alpha_{hr}) + i|\chi_{hi}| \exp(i\alpha_{hi})\end{aligned} \tag{1}$$

for a reciprocal-lattice vector $\mathbf{h}$ ($h = 1/d$, where d is the lattice plane distance). In the two-wave approximation, in order for the non-trivial solution for the fundamental equation to exist, the following equation must be satisfied approximately:

$$\begin{aligned}(\xi_o - i\kappa_{oi})(\xi_h - i\kappa_{oi}) &= \kappa_{or}^2 \chi_h \chi_{-h}/4 \\ &= \kappa_{or}^2 \overline{\chi_h}^2 [u + i(1-u^2)^{1/2} \cos\delta]/4,\end{aligned} \tag{2}$$

where

$$\delta = \alpha_{hi} - \alpha_{hr}. \tag{3}$$

Parameters $\overline{\chi_h}$ and u are defined by

$$\overline{\chi_h} = (|\chi_{hr}|^2 + |\chi_{hi}|^2)^{1/2} \tag{4}$$

$$u = 1 - 2q \tag{5}$$

and

ISSN 0108-7673

$$q = |\chi_{hi}|^2/\overline{\chi_h}^2. \quad (6)$$

Equation (2) gives a so-called dispersion surface which is a hyperbola, as shown in Fig. 1, when there is no absorption ($\chi_{0i} = 0$). The inner hyperbola is denoted as branch 1 and the outer one as branch 2. The other parameters in Fig. 1 are the same as in previous works by Fukamachi & Kawamura (1993) and Fukamachi *et al.* (1995).

A parameter W which expresses a deviation from an exact Bragg condition is given by

$$W = -X \sin 2\theta_B/(|\cos\theta_1 \cos\theta_2|^{1/2}\kappa_{or}\overline{\chi_h}). \quad (7)$$

Only σ polarization has been treated; π polarization can be treated in a similar manner by multiplying $|\cos 2\theta_B|$ with χ_{hr} and χ_{hi}.

3. Laue case

Consider a parallel planar crystal with the upper surface at $z = 0$ and the bottom one at $z = H$. In the two-wave approximation, two branches of the incident beam are excited when the incident beam $E_0 \exp(-2\pi i\mathbf{K}_0 \cdot \mathbf{r})$ enters the crystal surface.

By using the boundary conditions at $z = 0$, we obtain the reflection amplitude

$$R^{(j)} = (\overline{\chi_h}/\chi_{-h})(\cos\theta_1/\cos\theta_2)^{1/2}[W + ig' + (-1)^j L^{1/2}], \quad (8)$$

where $R^{(j)}$ is defined by

$$R^{(j)} = D_h^{(j)}/D_o^{(j)}. \quad (9)$$

In (8), the parameters L and g' are given by

$$L = (W + ig')^2 + [u + i(1 - u^2)^{1/2}\cos\delta] \quad (10)$$

and

$$g' = g \sin\theta_B \cos\beta/|\cos\theta_1 \cos\theta_2|^{1/2} \quad (11)$$

with

$$g = g_0 q^{1/2} \quad (12)$$

$$g_0 = \chi_{0i}/|\chi_{hi}|. \quad (13)$$

Here

$$D_o^{(j)} = [1 + (-1)^{j-1}(W + ig')/L^{1/2}]E_0/2 \quad (14)$$

and

$$D_h^{(j)} = (-1)^j(E_0/2)(\overline{\chi_h}/\chi_{-h})(\cos\theta_1/\cos\theta_2)^{1/2} \times [|L^{1/2}|^2 - (W + ig')^2]/L^{1/2}. \quad (15)$$

The wave field of branch j is expressed as

$$\begin{aligned} I^{(j)}(\mathbf{r}) &= |D^{(j)}(\mathbf{r})|^2 \\ &= |D_o^{(j)} \exp(-2\pi i\mathbf{k}_o^{(j)} \cdot \mathbf{r}) + D_h^{(j)} \exp(-2\pi i\mathbf{k}_h^{(j)} \cdot \mathbf{r})|^2 \\ &= |D_o^{(j)}|^2 \exp(4\pi k_{ozi}^{(j)} z)[1 + |R^{(j)}|^2 \\ &\quad + 2|R^{(j)}| \cos(2\pi\mathbf{h} \cdot \mathbf{r} - \omega^{(j)})]. \end{aligned} \quad (16)$$

Here $\omega^{(j)}$ is the phase angle given by

$$R^{(j)} = |R^{(j)}| \exp(i\omega^{(j)}). \quad (17)$$

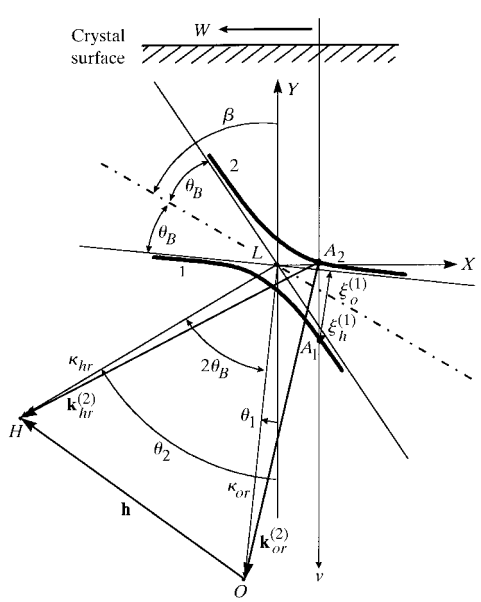

Fig. 1. Schematic diagram of dispersion surface for $q = 0$ and $\chi_{hi} = 0$ (thick solid lines).

3.1. *Symmetric Laue case for $q = 0$ ($\chi_{0i} \neq 0$)*

For a multiatomic crystal, the relation $q = 0$ holds if $\chi_{hi} = 0$ even when $\chi_{0i} \neq 0$. For a monoatomic crystal, on the other hand, $\chi_{hi} = 0$ holds only when $\chi_{0i} = 0$. In the following, we assume the former case.

From (8), the reflection amplitude $R^{(j)}$ is given by

$$R^{(j)} = [W + (-1)^j(W^2 + 1)^{1/2}]\exp(i\alpha_{hr}). \quad (18)$$

When $\alpha_{hr} = \pi$, $\omega^{(1)}$ is always zero and $\omega^{(2)}$ is π.

The wave field for $W = 0$ is

$$\begin{aligned} I^{(j)}(x) &= |D^{(j)}(x)|^2_{W=0} \\ &= (|E_0|^2/2)\exp(-\mu z/\cos\theta_B) \\ &\quad \times [1 + (-1)^{j-1}\cos(2\pi x/d)], \end{aligned} \quad (19)$$

where the x axis is taken in the direction of the reciprocal-lattice vector $\mathbf{h}$ and μ ($= -2\pi\kappa_{or}\chi_{0i}$) is the mean absorption coefficient. The last term in equation (19) expresses a standing wave with the period of the interlattice distance d. When $\alpha_{hr} = \pi$, the wave of branch 1 has an antinode at the lattice plane, while the wave of branch 2 has a node at the lattice plane as shown in the upper-middle part of Fig. 2. On the other hand, when $\alpha_{hr} = 0$, $\omega^{(1)} = \pi$ and $\omega^{(2)} = 0$ and the situation is reversed: the wave of branch 1 has a node and that of branch 2 has an antinode at the lattice plane.

Table 1. *The phase factor ω for $W = -1$, 0 and 1 in the symmetric Laue and Bragg cases*

		Symmetric Laue case			Symmetric Bragg case (semi-infinite)		
	Branch	$W = -1$	$W = 0$	$W = 1$	$W = -1$	$W = 0$	$W = 1$
$q = 0$ ($\alpha_{hr} = \pi$)	1	0	0	0	$-\pi$	$-\pi/2$	0
	2	π	π	π			
$q = 1$ ($\alpha_{hi} = \pi$)	1	$-\pi/2$	0	$\pi/2$	1.288π†	π	0.712π†
	2	$3\pi/2$	π	$\pi/2$			

† Numerically obtained.

Table 2. *The damping factor of the wave field given by equation (15) at $W = -1$, 0 and 1 for two branches in the symmetric Laue case*

	Change of term $\exp(4\pi k_{ozi}^{(j)} z)$ for the symmetric Laue case		
$q = 1$, branch	$W = -1$	$W = 0$	$W = 1$
1	$\exp(-\mu z/\cos\theta_B)$	$\exp(-2\mu z/\cos\theta_B)$	$\exp(-\mu z/\cos\theta_B)$
2	$\exp(-\mu z/\cos\theta_B)$	1	$\exp(-\mu z/\cos\theta_B)$

Note that in this case ($q = 0$) we cannot see the anomalous absorption and the anomalous transmission, though the absorption is included.

3.2. *Symmetric Laue case for $q = 1$*

$R^{(j)}$ in this case is given by

$$R^{(j)} = -i[W + (-1)^j (W^2 - 1)^{1/2}] \exp(i\alpha_{hi}), \qquad (20)$$

where we put $\alpha_{hi} = \pi$. For $W = \pm 1$, the phase angles are the same for branches 1 and 2: $\omega^{(j)} = -\pi/2$ for $W = -1$ and $\omega^{(j)} = \pi/2$ for $W = 1$. For $-1 < W < 1$, the phase angles are different for branches 1 and 2: $\tan\omega^{(1)} = W/(1 - W^2)^{1/2}$ and $\tan\omega^{(2)} = -W/(1 - W^2)^{1/2}$. [Note that the phase angles alter when $\alpha_{hi} = 0$: $\omega^{(j)} = \pi/2$ for $W = -1$, $\omega^{(j)} = -\pi/2$ for $W = 1$, and $\tan\omega^{(1)} = -W/(1 - W^2)^{1/2}$ and $\tan\omega^{(2)} = W/(1 - W^2)^{1/2}$ for $-1 < W < 1$.]

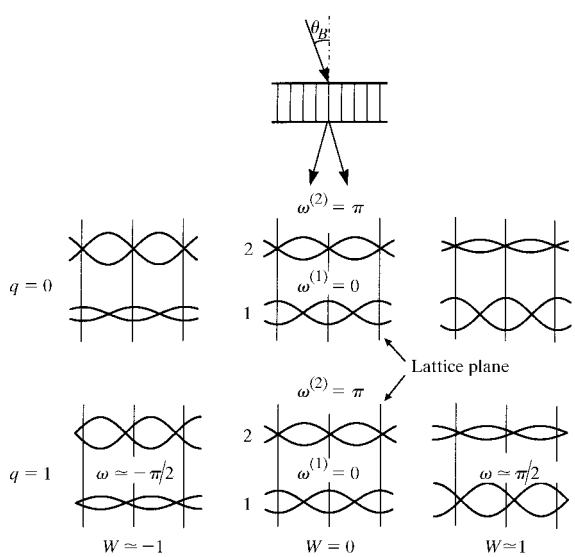

Fig. 2. Standing waves in the Laue case.

The values of the phase angles are shown in the left half of Table 1 for $W = -1$, 0 and 1 in the cases of $q = 0$ and 1. In Table 2, the damping terms $\exp(4\pi k_{ozi}^{(j)} z)$ in equation (16) are shown for $W = -1$, 0 and 1. For $|W| \geq 1$, waves of both branches 1 and 2 suffer the mean absorption of $\exp(-\mu z/\cos\theta_B)$. At $W = 0$, a wave of branch 1 has an absorption coefficient that is twice the size of the mean absorption coefficient (anomalous absorption), while the wave of branch 2 suffers no absorption (anomalous transmission). It is well known that a branch 1 wave ($\omega^{(1)} = 0$) has an antinode at a lattice plane and suffers anomalously strong absorption, while a branch 2 wave ($\omega^{(2)} = \pi$) has a node at a lattice plane and suffers anomalous transmission, as pointed out by Batterman & Cole (1964).

The strengths of the wave field $I^{(j)}(x)/|E_0|^2$ at point x near the surface ($sz = 10^{-5}$) are shown in Fig. 3(a) for branch 1 and in Fig. 3(d) for branch 2. Here the parameter s is defined as

$$s = \pi\kappa_{or}|\chi_{hi}|/\cos\theta_B. \qquad (21)$$

Most wave fields $I^{(j)}(x)$ diverge at $|W| = 1$ for any value of sz, as shown in Figs. 3(a)–(f). However, the total wave field $|D^{(1)}(x) + D^{(2)}(x)|^2/|E_0|^2$ does not diverge at any value of W, as shown in Figs. 3(g)–(i). This point will be discussed in detail in a separate paper.

At a lattice plane ($x = 0$), $I^{(1)}(0)/|E_0|^2$ increases when W increases from -2 to -1. It diverges at $W = -1$ and $W = 1$. It has a local minimum of 1 at $W = 0$. At the middle point between two adjacent planes ($x = d/2$), $I^{(1)}(d/2)$ shows similar variation except that it has a local minimum of 0 at $W = 0$. At a point $x = d/4$, $I^{(1)}(d/4)/|E_0|^2$ decreases from the maximum to a local minimum when W changes from -1 to 1, and becomes 1 for large W. At a point $x = 3d/4$, $I^{(1)}(3d/4)$ varies in

the opposite way to $I^{(1)}(d/4)$. The variations with respect to W for branches 1 and 2 are interchanged at $x = 0$ and $x = d/2$: $I^{(1)}(0, W) = I^{(2)}(d/2, -W)$ and $I^{(2)}(0, W) = I^{(1)}(d/2, -W)$. The variation of branch 1 at $x = d/4$ is just the opposite to that of branch 2 at $x = 3d/4$: $I^{(1)}(d/4, W) = I^{(2)}(3d/4, -W)$ and $I^{(1)}(3d/4, W) = I^{(2)}(d/4, -W)$.

In order to determine the relation of these standing waves to the Borrmann effect, we calculate the strength of the wave field inside the crystal. The damping term in (16) is

$$4\pi k_{ozi}^{(j)} z = \begin{cases} 2szg & (|W| \geq 1) \\ 2sz[g + (-1)^j (1 - W^2)^{1/2}] & (|W| < 1). \end{cases} \tag{22}$$

The wave field $I^{(1)}(0, W = 0)$, which has the antinode at the lattice plane, decreases rapidly when sz increases

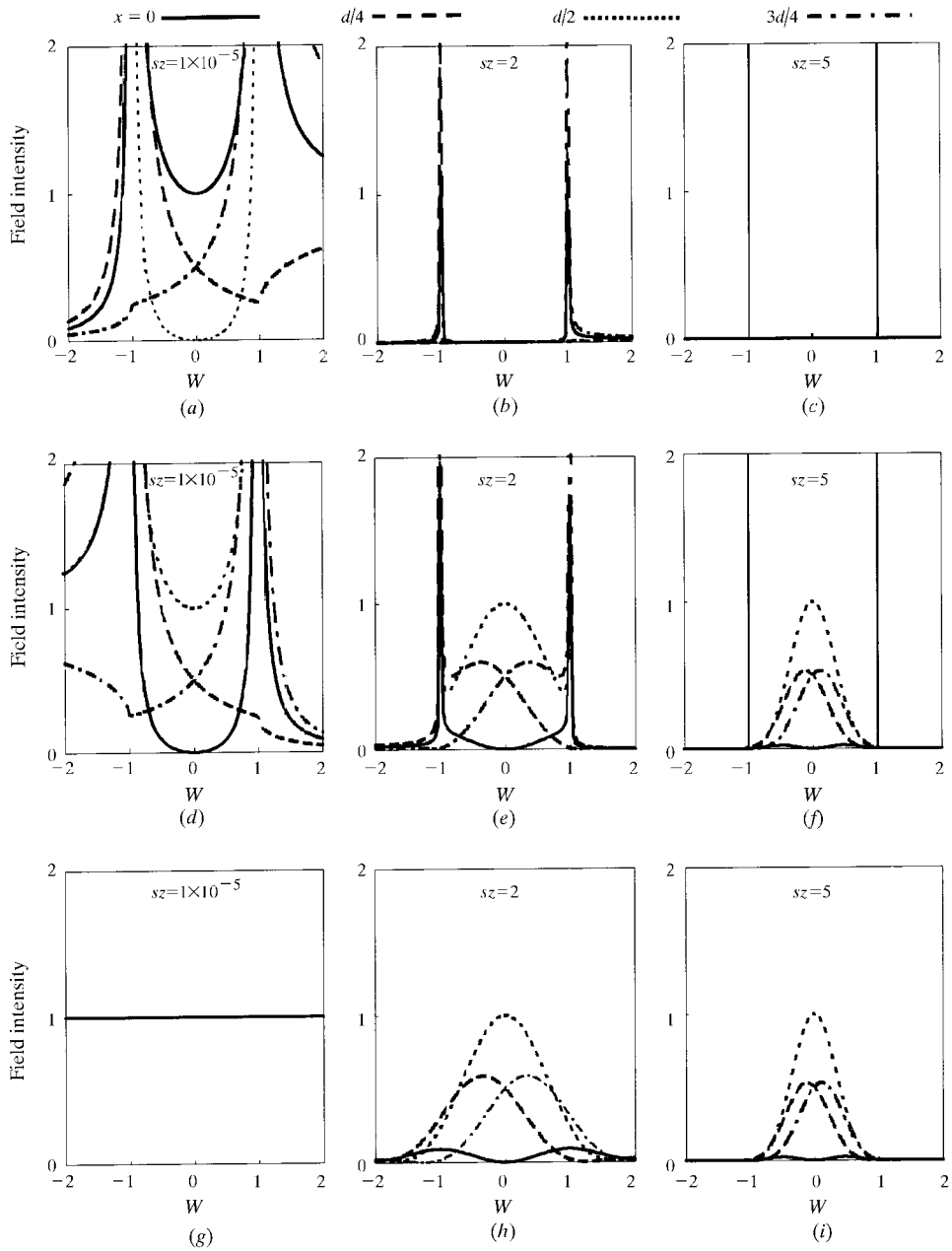

Fig. 3. Change of wave field $I^{(j)}(x)/|E_0|^2$ for $x = 0$ (solid line), $d/4$ (dashed line), $d/2$ (dotted line) and $3d/4$ (dash-dotted line) in the symmetric Laue case for $q = 1$, $g_0 = -1$ and $\alpha_{hi} = \pi$. Branch 1: (*a*) $sz = 1 \times 10^{-5}$, (*b*) $sz = 2$ and (*c*) $sz = 5$. Branch 2: (*d*) $sz = 1 \times 10^{-5}$, (*e*) $sz = 2$ and (*f*) $sz = 5$. Total field: (*g*) $sz = 1 \times 10^{-5}$, (*h*) $sz = 2$ and (*i*) $sz = 5$. Note that there is no divergence in the total field.

from 1×10^{-5} to 2 and 5 (Figs. 3*a–c*) for $g_0 = -1$. The wave field $I^{(2)}(d/2, W = 0)$, on the other hand, does not change at all as sz increases (Figs. 3*d–f*).

4. Bragg case

In the Bragg case for a semi-infinite crystal, one branch that gives rise to decreasing intensity into the crystal is chosen. The amplitude D_h is expressed by

$$D_h = (\overline{\chi_h}/\chi_{-h})(\cos\theta_1/|\cos\theta_2|)^{1/2} \times [-(W + ig') \pm B^{1/2}]E_0, \quad (23)$$

where B is given by

$$B = (W + ig')^2 - [u + i(1 - u^2)^{1/2}\cos\delta]. \quad (24)$$

The wave field of branch j in this case has exactly the same form as equation (16).

4.1. *Symmetric Bragg case for $q = 0$ ($\chi_{0i} = 0$ or $\chi_{0i} \neq 0$)*

The dispersion surface when $q = 0$ with $\chi_{0i} \neq 0$ in the symmetric Bragg case is given by

$$(X\cos\theta_B)^2 - (Y'^2 - Z'^2)\sin^2\theta_B - \kappa_{oi}^2 = \kappa_{or}^2|\chi_{hr}|^2/4 \quad (25a)$$

$$Y'Z'\sin^2\theta_B + \kappa_{oi}X\cos\theta_B = 0. \quad (25b)$$

The dispersion surface is depicted in Fig. 4 for $g = 0$ ($\chi_{0i} = 0$) and $g = -0.1$ ($\chi_{0i} \neq 0$). The thick solid and the thick dashed lines show the real and the imaginary parts, respectively, of the physically allowed dispersion surface when $g = -0.1$. The thin solid and the thin dashed lines are the real and imaginary parts, respectively, of the dispersion surface when $g = 0$ ($\chi_{0i} = 0$). When χ_{0i} is not zero, Y' and Z' are not zero for $|W| = 1$, which is quite different from the dispersion surface when $\chi_{0i} = 0$.

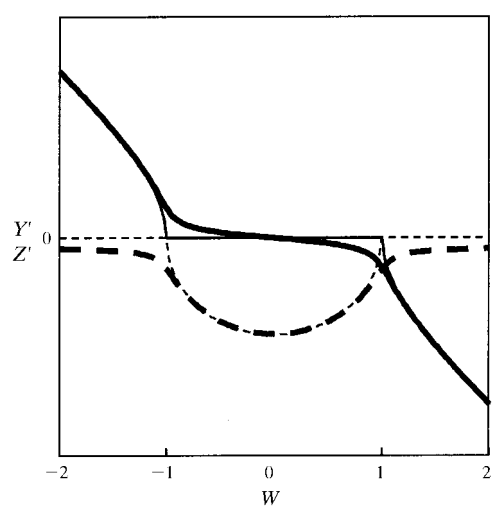

Fig. 4. Dispersion surface in the symmetric Bragg case for $q = 0$. The thick solid and the thick dashed lines show the real and the imaginary parts, respectively, of the physically allowed dispersion surface when $g = -0.1$ ($\chi_{0i} \neq 0$); the thin solid and the thin dashed lines are the real and imaginary parts of the dispersion surface when $g = 0$ ($\chi_{0i} = 0$).

The reflection coefficient R is given by

$$R = -\{W + ig' \pm [(W + ig')^2 - 1]^{1/2}\}\exp(i\alpha_{hr}) \quad (26)$$

where we put $\alpha_{hr} = \pi$. Note that phase angle ω becomes $-\pi/2$ when $W = 0$. The phase angles for $W = -1, 0$ and 1 are given in the right half of Table 1. In the limit of $g = 0$ ($\chi_{0i} = 0$), the phase angle ω becomes $-\pi$ for $W = -1$ and zero for $W = 1$. The forms of the standing wave for these values of W in the case of $g = 0$ are shown in the upper part of Fig. 5. When $W = -1$, the standing wave has its node at a lattice plane. When $W = 1$, on the other hand, the standing wave has its antinode at a lattice plane. This result is the same as obtained by Batterman & Cole (1964).

The variations of the wave field $I(x)/|E_0|^2$ in the range $-2 < W < 2$ are shown in Fig. 6. At a lattice plane $x = 0$, $I(0)$ decreases when W changes from negative infinity to -1 and shows the minimum at $W \simeq -1$. It increases when W changes from -1 to 1 and shows the maximum at $W \simeq 1$. Then it decreases monotonically. At a plane $x = d/2$, $I(d/2)$ shows just the opposite variation to $I(0)$. At $x = d/4$, $I(d/4)$ decreases when W changes from -1 to 0, showing the minimum at $W = 0$, and increases when W changes from 0 to 1. At $x = 3d/4$, $I(3d/4)$ shows just the opposite variation to $I(d/4)$.

4.2. *Symmetric Bragg case for $q = 1$*

When $g_0 = -1$, the equations of the dispersion surface are given by

$$Y'Z'\sin^2\theta_B = -\kappa_{or}|\chi_{hi}|X\cos\theta_B/2 \quad (27a)$$

$$(Y'\sin\theta_B)^2 - (Z'\sin\theta_B)^2 - (X\cos\theta_B)^2 = 0. \quad (27b)$$

Since $X = Y' = Z' = 0$ satisfies (27*a*) and (27*b*), two dispersion surfaces of hyperbola touch each other at $W = 0$ where the total reflection is observed (Kato,

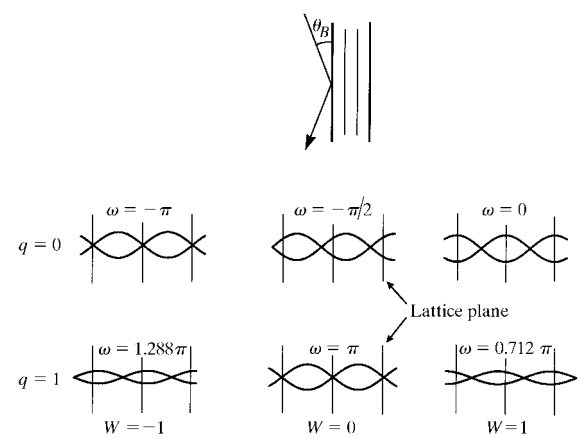

Fig. 5. Standing waves in the Bragg case.

1992; Fukamachi & Kawamura, 1993; Fukamachi *et al.*, 1995). The phase ω varies from 1.288π to π and 0.712π when W changes from -1 to 0 and 1 (Table 1). The wave fields $I(x)/|E_0|^2$ at $x = 0$, $d/4$, $d/2$ and $3d/4$ are given in Fig. 7 as a function of W for $\alpha_{hi} = \pi$. The wave field $I(0)$ shows a minimum of 0 at $W = 0$. On the other hand, $I(d/2)$ shows a maximum at $W = 0$. The standing waves for $W = -1$, 0 and 1 are shown in the lower part of Fig. 5. The standing wave for $W = 0$ has a node at a lattice plane $x = 0$ and an antinode at the midpoint between lattice planes $x = d/2$. This is quite different from a standing wave in the case of $q = 0$, which does not have either a node or an antinode at a lattice plane or at the midpoint between the planes.

5. Summary

We have studied standing waves from X-ray dynamical diffraction, especially when the real component of the X-ray polarizability χ_{hr} is zero and the imaginary component χ_{hi} is not zero ($q = 1$). We have used the strength of the electric displacement $I^{(j)} = |D^{(j)}(\mathbf{r})|^2$ for branch j to study the wave field, and analysed the cause of anomalous absorption and anomalous transmission in the Laue case by considering the forms of the standing waves.

In the symmetric Laue case, by tuning X-ray energy very close to an absorption edge of an atom in a crystal, we have a condition when $\chi_{hr} \neq 0$, $\chi_{hi} = 0$ and $\chi_{0i} \neq 0$, *i.e.* $q = 0$ in terms of the present parameter. In this case, the standing wave of branch 1 has an antinode at the lattice plane and the wave of branch 2 has a node at the plane. It is noted that, since $\chi_{hi} = 0$ ($\chi_{0i} \neq 0$), there is no anomalous absorption nor an anomalous transmission effect, which is quite different from the situation when $\chi_{hi} \neq 0$.

When the real component χ_{hr} is zero and the imaginary component χ_{hi} is nonzero ($q = 1$), the phase factor $\omega^{(1)}$ of branch 1 changes from $-\pi/2$ to 0 and $\pi/2$ by increasing W from -1 to 0 and 1. At $W = 0$, the wave of branch 1 has an antinode at the lattice plane and an absorption coefficient that is twice the size of the normal one. In contrast, the phase factor of the wave of branch 2 changes in the opposite way. The wave of branch 2 has a node at the lattice plane and the wave field does not decrease, which results in anomalous transmission effects for both the diffracted and the transmitted beams.

In the symmetric Bragg case, as is well known, when $q = 0$ and $\chi_{0i} = 0$, the total reflection occurs for $-1 \leq W \leq 1$. The phase factor ω changes from $-\pi$ to $-\pi/2$ and 0 when W changes from -1 to 1. When $q = 1$, the total reflection occurs only at $W = 0$. The standing wave in this case has a node at the lattice plane.

X-ray standing waves have been used to determine an impurity site in a bulk or an adsorbed-atom site on a crystal surface by measuring fluorescent X-rays or secondary electrons excited by the incident X-rays. Most of these experiments are performed in a reflection mode, *i.e.* in the Bragg case when the absorption is weak ($g \simeq 0$) (Zegenhagen, 1993). We have shown that a similar variation of the standing wave is expected in the Laue case when the real component of X-ray polarizability, χ_{hr}, is zero, with the imaginary part, χ_{hi}, nonzero ($q = 1$). Especially at $q = 1$, the standing wave can be utilized to determine an impurity site in a bulk because the transmitted intensity is high due to anomalous transmission and a thick crystal can be used in the

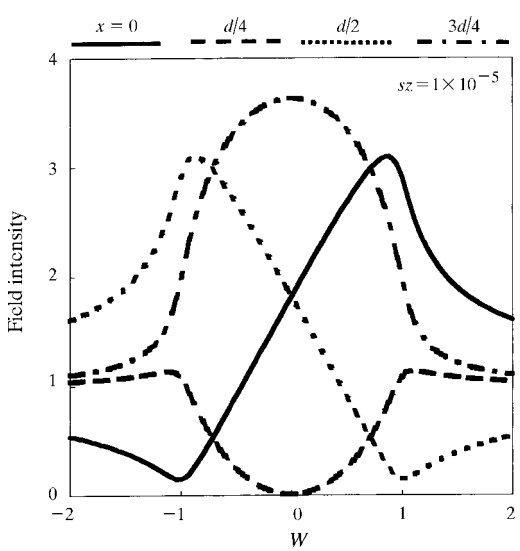

Fig. 6. Change of the wave field $I(x)/|E_0|^2$ for $x = 0$ (solid line), $d/4$ (dashed line), $d/2$ (dotted line) and $3d/4$ (dash-dotted line) in the symmetric Bragg case for $q = 0$, $g = -0.1$ and $\alpha_{hr} = \pi$.

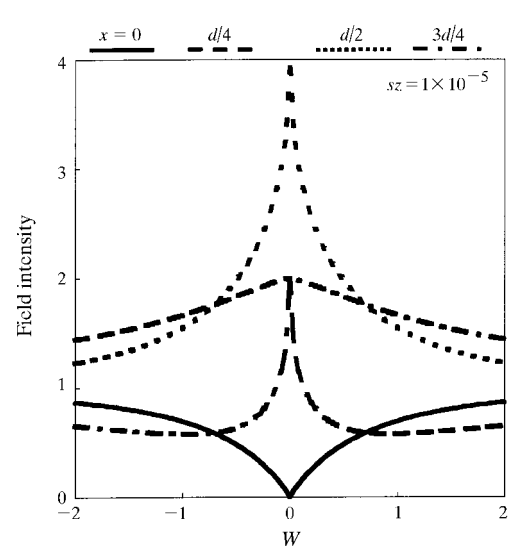

Fig. 7. Change of the wave field $I(x)/|E_0|^2$ for $x = 0$ (solid line), $d/4$ (dashed line), $d/2$ (dotted line) and $3d/4$ (dash-dotted line) in the symmetric Bragg case for $q = 1$, $g_0 = -0.1$ and $\alpha_{hi} = \pi$.

experiment. The higher transmitted intensity also makes the measurement easier and more accurate. In addition, samples of a wider range of thickness can be used in the experiments, which should be an advantage in preparing the sample.

References

Batterman, B. W. & Cole, H. (1964). *Rev. Mod. Phys.* **36**, 681–717.
Fukamachi, T. & Kawamura, T. (1993). *Acta Cryst.* A**49**, 384–388.
Fukamachi, T., Negishi, R. & Kawamura, T. (1994). *Acta Cryst.* A**50**, 475–480.
Fukamachi, T., Negishi, R. & Kawamura, T. (1995). *Acta Cryst.* A**51**, 253–258.
Fukamachi, T., Negishi, R., Yoshizawa, M., Ehara, K., Kawamura, T., Nakajima, T. & Zhao, Z. (1993). *Acta Cryst.* A**49**, 573–575.
Kato, N. (1992). *Acta Cryst.* A**48**, 829–833.
Zegenhagen, J. (1993). *Surf. Sci. Rep.* **18**, 199–271.